hybrid Simulations of Interstellar Pick-up Ion Acce era ion at the Solar Wind Termination Shock

P. C Liewer, Sharadini Rath[1], 11.1". Goldstein,

Jet Propulsion Laboratory, California in.vtitulc of Technology,

Pasadena, CA 91109

Abstract

1 Iybrid (kinetic ion/fluid electron) simulations have been used to study self-consistently the injection and initial stages of acceleration of interstellar pick-up ions at the solar wind termination shock. Results are presented from one-dimensional simulations of high Mach number oblique (40°--50°) shocks with a 10% population of interstellar pick-up hydrogen. In these simulations, the pick-up ions, the solar wind ions, the shock fields and the waves are all treated self-consistently. Pick-up ions reflected by the shock excite large amplitude ($\Delta B/B$ - 0.3) upstream magnetosonic waves. These waves, in turn, scatter the pick-up hydrogen, as expected in the diffusive shock acceleration process. The spectrum of excited waves broadens in time. We find that, for the parameters studied, the terminat ion shock efficiently injects ant! accelerates the interstellar pick-up hydrogen, anti thus this work represents a microscopic verification of this anomalous cosmic ray injection mechanism. Comparison of injected fluxes from the. simulations with Voyager fluxes extrapolated to the termination shock suggests that injection at the termination shock is probably greater than injection by interplanetary shocks. A study of accelerated pick-up ion orbits shows that the energy gain comes predominantly from shock drift acceleration in the shock front, with the upstream waves aiding the acceleration by allowing multiple encounters with the shock.

.

[1]Present address: International Center for Theoretical Physics, 34014 Trieste, Italy

1. Introduction

It has been hypothesized that anomalous cosmic rays (20-300 MeV) may result from the acceleration of interstellar pick-up ions injected at the solar wind termination shock [Pesses et al., 1981; Jokipii, 1986, 1990]. Interstellar pick-up ions enter the heliosphere as neutrals. They are ionized and picked up by the solar wind which carries them back out to the termination shock. The interstellar neutrals (~20 km/see) have a large velocity relative to the solar wind (V_{SW}~400 km/sec) and hence these pick-ups have a much larger energy in the solar wind frame (~$^1/_2 m V_{SW}^2$) than the background solar wind ions. 'J'bus, they form a natural higher energy "seed" population for injection and acceleration at the termination shock. The largest pick-up component is expected to be hydrogen, representing over 10% of the solar wind ion density if the termination shock is beyond 50 AU. Recently, Gloeckler et al. [1993] have made the first observat ions of inter stellar pick-up hydrogen,

]ons are accelerated at collisionless shocks pr imarily by two processes [see reviews byForman and Webb, 1985 and Jones and Ellison, 1991]: shock drift acceleration anti first order Fermi acceleration. In shock drift acceleration, an ion gains energy via its $\mathbf{VB}$ drift at the shock front in the direction of the convective $\mathbf{vxB}$ electric field. in this process, the ion travels along the shock front and gains energy continuously, in first order Fermi acceleration, an ion gains energy by scattering between converging magnetic fluctuations upstream anti downstream of the shock. For parallel shocks, with no average jump in the magnetic field at the shock, Fermi acceler at ion is expected to dominate, whereas in more oblique or quasi-perp endicular shocks, shock drift acceleration is expected to dominate [Jokipii, 1987]. The role of shock drift acceler ation has been further clarified by the work of Decker and Vlahos [1986a,b] and Decker [1988] in calculations of test particle orbits in specified (i.e., not self-consistent) shock and magnetic fluctuation fields.

Much of the work on ion acceleration at shocks uses the standard convection-diffusion cosmic ray transport equation which contains both shock drift and Fermi acceleration [Jokipii, 1982, 1990; Jones and Ellison, 1985]. Diffusive theory provides a

description of ion acceleration on macro, e.g., heliospheric, spatial and temporal scales. It is valid for isotropic distribution functions and particles with velocities much greater than any convective speeds in the problem. Diffusive theory can be used to describe the acceleration of such suprathermal ions in the heliosphere to cosmic ray energies for which the acceleration processes takes place on the 100 AU spatial scale and year time scale (see e.g. Jokipii [1990]). in diffusive transport models, the. microscopic fields of the heliosphere and the diffusion coefficient, which includes the wave scattering from small scale fluctuations, are specified (using results from other theories and/or models) and an assumed energetic seed population is "injected." Because it provides a [macroscopic description, results from diffusive cosmic ray transport models can be compared directly with cosmic ray observations. The theory, however, cannot be used to model the injection and acceleration of the freshly picked up interstellar ions because of their low energy and non-isotropic distribution.

Here, we use the complementary technique of hybrid particle simulation to study the injection and acceleration of freshly picked up interstellar ions at the solar wind termination shock. In hybrid simulations, scattering and diffusion result directly from the wave-particle interactions in the simulations. Self-consistent hybrid simulations have been used previously by Giacalone et al. [1992, 1993] and Scholer [1990] to study the acceleration of thermal ions in parallel or nearly parallel shocks ($\theta_{Bn} < 20^o$ where θ_{Bn} is the angle between the magnetic field and the shock normal). Burgess (1987) studied shock drift acceleration in oblique shocks of suprathermal test particles in 1-D hybrid simulations. We have extended this previous work to study the acceleration of the energetic pick-up ion "seed" population in oblique ($\theta_{Bn} = 30^o$-60^o) shocks. The suprathermal pick-up ions in our simulations are not "test particles" as in Burgess (198'/), but are treated self-consistently and have a major effect on both the macroscopic and microscopic fields. In addition, we have studied the evolution of the. spectrum of the upstream waves generated self-consistently by the reflected pick-up ions; no upstream waves are injected.

Wc find that, for' the oblique shocks studied, pick-up ions are efficiently injected and accelerated by the. termination shock. For a strong shock (M_A = 8), about 40% of the incident pick-up ion flux was init ially reflected. From a study of the accelerated pick-up ion orbits, we find that the energy gains come predominantly from shock drift acceleration in the shock front, with the upstream waves playing the crucial role of al lowing the pick-up ions to have multiple encounters with the shock. For a strong shock, many icms are observed to be accelerated to about 30 keV, which is 50 times their initial energy. 1 Iybrid simulations can provide only a micro-scale. description of the injection and initial acceleration of interstellar pick-up ions. Computer resources limit spatial scales to fractions of an AU and time scales of tens of hours. 1 lowever, the energetic ion fluxes from such models can then be used as input to models bawd on the convection-diffusion cosmic ray transport equat ion which can then follow the acceleration process to the obser ved anomalous cosmic ray energies (20-300 MeV).

We have also addressed the question of whether the fluxes injected into the global heliospheric shock acceleration process at the termination shock as computed by the simulations are greater than fluxes injected by interplanetary shocks as obser ved by Voyager. For this comparison, we have used Voyager low-energy charged particle (1 .ECP) flux spectra data from shock acceleration events (Gold et al., 1988), measured at about 15 -20 AU, extrapolated adiabatically to 80 AU (the location of the termination shock in our simulations) and compared the flux spectra in the energy range j-1()() keV. We find that the simulation fluxes are about 1-2 orders of magnitude larger than the measured fluxes extrapolated to 80 AU in this energy range. Although there is considerable uncertainty introduced by comparing fluxes from two intermittent events at different locations, the results indicate that the termination shock is probably the primary injection site for the anomalous cosmic ray component.

The paper is organized as follows. in Section 2, the simulation model and parameters are described and the angular range of validity of the model discussed. in

Section 3, simulation rt'suits are presented and analyzed and compared with Voyager observations. The results are summarized and discussed in Section 4.

2. Simulation Model and Parameters

The hybrid simulation model used here, as well as the assumed termination shock parameters, have been described in Liewer et al. [1993]. The code is based on the hybrid code of Winske and Leroy 11985J and uses a first-order accurate time stepping algorithm. For the studies here, the code was modified to include a second ion species, the interstellar pick-up ions, which are initialized with a non-thermal distribution in velocity space. Both ion species are treated in a fully self-consistent manner since the. macroscopic and microscopic fields are strongly influenced by both. To get reasonable statistics for the accelerated pick-up ions, wc use relatively more simulation particles to represent the pick-ups than the thermal ions and weight the pick-up and thermal ion simulation particles accordingly when computing the local density, momentum and current from the simulation particles. For the cases presented here, 1/3 of the total simulation particles are pick-up ions even though the pick-ups represent 1()% of the total density,

For most of the simulations, we assume, as in Liewer et al. [1993], a spherical shell velocity distribution with zero width and a radius equal to the solar wind velocity co-moving with the solar wind ions. To test the effect of the assumed distribution on the injection process, we have also run simulations using an adiabatically cooled pick-up ion distribution, $f(v) \propto v^{-3/2}$ [Möbius et al., 1988].

In our model, the simulation is done in the downstream frame. ions are injected from the left of the simulation box and reflect off the right wall. The shock forms at the right wall and propagates to the left. Reflected ions that reach the left wall are absorbed. In the simulations below, $\omega_{pi}/\omega_{ci} = 7000$," $\beta_e = 0.5$, $\beta_i = 0.2$, and the fractional density of the pick-up hydrogen is $n_0^p/n_0 = 10\%$ where n_0 is the initial total density and n_0^p is the initial hydrogen pick-up ion density. These numbers, plus the angle and Mach number,

characterize the shocks completely and represent values expected for a solar wind termination shock at ~80 AU [Liewer et al., 1993].

The code uses dimensionless units with length normalized to c/ω_{pi} where ω_{pi} is the ion plasma frequency ($\omega_{pi}^2 = 4\pi n_0 e^2/m_p$ with m_p the proton mass), and velocities are normalized to c, the sped of light. Variation is allowed only in the x (shock propagation) direction and the initial magnetic field is in the x-z plane. The simulation of particle acceleration to high energies requires very large system sizes and long run times and, thus, large amounts of CPU time. The computations were performed using 32 processors of the **512** processor Intel Delta Touchstone parallel computer at Caltech and ran about 12 hours. Typical runs had a time step of $0.025\omega_{ci}^{-1}$, a system length of 3500 c/ω_{pi} with 7000 grid points and 1 million particles and ran for 20,000 time steps. For solar wind parameters at about 80 AU, the time step corresponds to about 6 sec and $c/\omega_{pi} \approx 7000$ **km.** in calculating the injected differential fluxes (flux per unit energy, ions/cm^2-sec-keV), a plasma density of $n_0 = 9.4 \times 10^{-4}$ cm^{-3} was used, obtained by extrapolating a density of $n_0 = 6$ cm^{-3} at earth to 80 AU.

The processes studied in this work -- injection and acceleration at shocks -- are very sensitive to the shock angle θ_{Bn}. Oblique shocks generally allow more reflected pick-up ions to move back upstream to both excite waves and to be further scattered and accelerated than do quasi-perpendicular shocks. Our one-dimensional hybrid simulations, as well as simple estimates, show that to get significant ion reflection and reflected-ion driven upstream waves, the. shock angle must be less than about 60° [Liewer et al., 1993]. Acceleration in oblique shocks is of particular interest because the importance of shock drift acceleration relative to first order Fermi acceleration increases with increasing shock angle and magnetic field jump, and the rate of acceleration also increases [Jokipii, 1987]. We have studied the injection and acceleration processes for a range of oblique shock angles $\theta_{Bn} = 30° - 60°$.

Recently, Jokipii et al.[993] have found that one- and two- dimensional hybrid

simulations cannot be used to study shock acceleration in quasi-perpendicular shocks because of the inhere'nt neglect of cross field diffusion in one- and two-dimensional models. It may be that if cross field diffusion effects were present in the 1D hybrid simulations, significant injection might also occur for $\theta_{Bn} > 60^o$. Note that the diffusion coefficients are free parameters in diffusion/convection models only. in hybrid simulation models, the diffusion coefficients can not be specified because the scattering results directly from the wave-particle interaction in the simulations. One- and two-dimensional simulations with "ad hoc" cross-field diffusion might give some information cm this issue (see, e.g., *Giacalone et al. [1994],* but ultimately fully three-dimensional simulations will be necessary to resolve this issue.

Since c1oss field diffusion is not present in one-dimensional hybrid models such as that used here, we address the question of the range of angles for which this neglect might have a significant effect. Although difficult to quantify, we present here one simple estimate. The relevant diffusion coefficient for shock acceleration is the component

$$K_{xx} = K_{||}\cos^2\theta + K_{\perp}\sin^2\theta$$

where $K_{\perp}$ and $K_{||}$ are the ion diffusion coefficients perpendicular anti parallel to the field respectively, x is the direction of the shock nor ma] and θ is the angle between the magnetic field anti the x axis; the acceleration rate is inversel y proportions] to K_{xx} [Jokipii, 1987]. '1'bus, we estimate that neglect of perpendicular transport will not become important until the neglected transport, $K_{\perp}\sin^2\theta$, becomes comparable to that retained, $K_{||}\cos^2\theta$. The unknown ratio $K_{\perp}/K_{||}$ will depend on the magnetic turbulence. Since the ratio is unknown in the vicinity of the termination shock, we estimate the effect for several assumed values. The largest upstream angle in the simulations presented was 500; the largest downstream angle was about 75°. Taking $K_{\perp}/K_{||} = 0.01$ (corresponding to a parallel diffusive step size 10 times the perpendicular diffusive step size), neglect of $K_{\perp}$ is a <14% effect ($K_{\perp}\sin^2\theta/K_{||}\cos^2\theta < 0.14$) for $\theta < 75^o$. Thus, neglect of $K_{\perp}$ will be a small effect for all angles in these simulations for $K_{\perp}/K_{||} \leq 0.01$ and neglect of cross field diffusion is justified.

If $K_\perp/K_\parallel = ().1$, then at $\theta \approx 50^o$ (the largest upstream angle in the simulations presented), neglect of $K_\perp$ might produce a 14% effect. However, for $\theta \approx 75^o$, the effects of perpendicular diffusion would dominate ($K_\perp \sin^2\theta/K_\parallel \cos^2\theta > 1$). If $K_\perp/K_\parallel \approx 1$, then the effects of perpendicular diffusion would dominate for $\theta > 45^o$ and neglect of cross field diffusion would clearly not be justified.

Since our 1 D hybrid models injects pick-up ions into the acceleration process only for $\theta_{Bn} < 60^o$, and since the termination shock is generally assumed to be quasi-perpendicular ($\theta_{Bn} \approx 90^o$), it is necessary to estimate the fraction of the time the shock angle will fall below 60^o in order to estimate the globally average injected flux. If the heliospheric magnetic field were the constant Parker spiral and the termination shock were spherical, the shock angle would fall below 60^o only within a degree or so of the heliospheric pole and thus the fraction of time in this range would be negligible. However, considerations of the variability in both the interplanetary magnetic field and the shock normal direction lead to a much larger, although rather uncertain, estimate.

Firstly, hourly averaged 1991 Pioneer magnetic data at 35 AU shows that the angle of the magnetic field itself is highly fluctuating and thus, even near the ecliptic, the angle between the field and the radial direction will at times be less than 60^o. From the 1991 Pioneer magnetic field data presented in Lieweer et al. [1993], we calculate that the angle between the field and the radial direction falls below 600 about 20% of the. time; it is not known how this number will extrapolate to6080 AU,

Secondly, only for a steady, spherically symmetric termination shock is the shock normal always in the radial direction, Hydrodynamic models show that if the very local interstellar medium (V1 .ISM) flow is supersonic as suggested in a recent study of the morphology of the VI .ISM by Frisch [1994], then the heliosphere has an external bow shock (see Baranov and Malama [1993] and references therein j anti the termination shock becomes bullet-shaped with the nose pointing into the VI .ISM flow. In this case, the shock normal is not radial over some portion of its surface. From a two-dimensional

axisymmetric calculation of such a "two-shock" heliosphere [Karmesin et al., 1995], we find that the shock normal is more than 30° from the radial direction (and thus $\theta_{Bn} < 60°$) over about 15% of the shock surface. The distortion of the shock from spherical, anti thus this percentage, will depend, of course, on the VLISM parameters which have a large uncertainty. Variability due to a non-spherical termination shock would lead to a non-uniform injection with more injection from the tail hemisphere than the nose hemisphere.

From these various considerations, a very crude estimate is that the shock angle will fall below 60° about 10-30%, of the time. Using the fact that in our model injection occurs only for $\theta_{Bn} < 60°$ and using the above estimate for the time spent in this range, the average injected flux at the termination shock will be lower than the simulation fluxes by a factor of about 3-5. We have studied the injection and acceleration processes for a range of shock angles $\theta_{Bn} = 30° - 60°$. Results are presented below for two angles, 40° and 50°, but the results are qualitatively similar over this range of oblique angles. It is important to note that if cross-field diffusion is large enough to allow significant injection for shocks with $\theta_{Bn} > 60°$, then injection of pick-up ions from quasi-perpendicular shocks might be more important than injection for oblique shocks studied here, since the termination shock will be quasi-perpendicular more often than it is oblique. Because of these considerations, our calculations may underestimate the rate of injection of pick-up ions at the termination shock.

3. Simulation Results

We will first present detailed results from two case studies, characterized by the angle θ_{Bn} between the magnetic field and the shock normal and the Alfven Mach number M_A (the ratio of the solar wind speed to the Alfven speed). Case 1 has $\theta_{Bn} = 40°$ and $M_A = 5$; Case 2 has $\theta_{Bn} = 50°$ and $M_A = 8$. In both simulations, as the shock propagates, the interstellar pick-up hydrogen ions are preferentially reflected by the shock as reported previously [Lee et al., 1993]. A counter-streaming ion cyclotron instability between these reflected pick-up ions and the background solar wind leads to large amplitude

upstream magnetosonic waves. These magnetic fluctuations are swept back towards the shock by the super-Alfvenic solar wind flow, thus creating the situation for first order Fermi acceleration. The pickup ions are observed to be further accelerated in these shock and waves fields. in these simulations, the waves and turbulence are generated by the shock, *i.e., no* waves are injected upstream.

.3.1 Case 1 (θ_{Bn}=40° *and MA = 5)*

1 'igure 1 shows results from the lower Mach number Case 1 at t imes early and late in the simulation. This Mach number corresponds to a solar wind speed of about 200 km/sec which might be expected if the solar wind flow was slowed by the galactic cosmic ray pressure. Figure 1 a shows results at t=150ω_{ci}^{-1}. In the top panel, the magnetic field component $B_y(x)$ vs. x (with B normalized to the upstream magnetic field magnitude B_0), *shows* a large amplitude upstream magnetosonic wave with peak amplitude, $\Delta B_y/B_0 \approx 0.5$. The second panel shows pick-up ion V_x *vs. x* phase space with only every 60th ion plotted. in this panel, the injected pick-up ion shell distribution is seen as the band of ions centered on $v_x/c = 5x10^{-4}$; *some* reflected pick-ups are evident as those with negative V_x. 'l'he third panel shows a subset of the pick-up ions, "energetic/reflected" pick-up ion phase space V_x vs. x, where "energetic/reflected" pick-ups are *upstream* ions with energy greater than 4 times the initial energy in the solar wind frame ($E_0 = {}^1/_2 m_p V_{sw}^2$ where Vs_w is the solar wind speed); all such ions are plotted. The magnetosonic wave structure seen in the B_y plot is clearly evident in the energetic/reflected ion phase space, confirming that it is indeed the reflected pick-up ions which are driving the upstream instability. These waves propagate upstream at roughly the Alfven speed, but arc convected back towards the shock by the M_A = 5 solar wind flow, In Fig. 1 b (t =550ω_{ci}^{-1}), the y component of the magnetic field $B_y(x)$, the total magnetic field amplitude |B(x)|, and "energetic/reflectcxl" pickup ion phase space V_x vs. x are shown, The wave amplitude is comparable to the val uc at the earlier time, but the waves appear to be much less monochromatic. Moreover, the energetic ion phase space shows much less structure, and higher energy ions are evident, indicating that

nonlinear mmvc.-scaltcring processes are playing a significant role.

Figure 2 shows the magnetic fluctuation spectra $P(k)=B^2(k)/8\pi$ VS. k, (with k in units of ω_{pi}/c) at the. same two times as in Fig. 1 integrated over a region extending 1024 c/ω_{pi} ahead of the shock. At the early time, the spectrum is peaked around the value $ck/\omega_{pi} \approx 0.12$. This is consistent with theoretical expectations for the beam-driven ion cyclotron instability which predicts $\omega - \mathbf{k}\cdot\mathbf{V_b} = k_{\|}(V_A - V_b) = -\omega_{ci}$. The beam velocity along the field, determined from plots of the reflected ion $v_\perp - v_\|$ phase space, is $V_b/V_A \approx 12$. With $k = k_{\|}/\cos\theta_{Bn}$, the predicted valued is $ck/\omega_{pi} \approx 0.12$ as observed. At later times, (he spectrum has clearly broadened, with more energy going into longer wave length modes. The broadening of the spectra] peak around O.12 presumably results from the broadening of the reflected pick-Lip ion beam observed in the reflected/energetic ion phase space in Fig. 1b, wit h the longer wavelength modes excited by the more energetic pick-up ions.

in order to understand better the shock acceleration process and the. relative role of wave scattering and shock drift acceleration, "orbits" of the most energetic ions were plotted. Two typical ion orbits are shown in Fig. 3 where an individual ion's energy (in the solar wind frame) is plotted as a function of its distance from the shock front $x-x_{shock}$ (negative values are upstream) where x is normalized to c/ω_{pi}. Here $E = v^2/c^2$ (*e.g.*, energy is normalized to $m_p c^2/2 = 4.7\times10^5$ keV) and the initial pick-up ion energy is $E_0 = \frac{1}{2}m_p V_{SW}^2 = .5\times10^{-7}$ (corresponding to 240 eV). The ion position and energy at the start of the simulation are at the bottom left end of the 01 bit curve. This type of plot clearly shows the energy gain from shock drift acceleration: the ion stays in the shock front ($x-x_{shock} \approx 0$) and gains energy continuously. Wave scattering causes the obser ved abrupt *decreases* in energ y because the waves are propagating away from the shock and the reflected ions are overtaking the waves. (In some cases, wave scattering causes an increase, in energy, indicating that some backward propagating waves have been excited.) 1 rom investigation of the orbit plots, wc concluded that both processes, wave scattering and shock drift acceleration, are important in accelerating pick-up ions at the termination shock. Wave

scattering is important because it allows the ions to have multiple encounters with the shock; the actually energy gain comes from the ion drift in the convective **vxB** shock electric field [Jokipii, 1982, 1987, 1990; Jones and Ellison, 1985].

From the study of 65 orbits of' the most energetic ions in Case 1, we found that acceleration resulted primarily from shock drift acceleration at the shock front, where the energy gained from shock drift acceleration in a single encounter was often much greater than the gain from simple specular reflection by the shock. Scattering from upstream waves was the dominant mechanism for returning, ions to the shock front, with downstream waves playing a smaller role. in many roses, ions stayed quite near to the shock (within $\sim 100\ c/\omega_{pi}$ or 5-20 ρ_i where., in our units, pi $= \omega_{pi}/\omega_{ci} E^{1/2} = 7000 E^{1/2}$) and shock drift acceleration led to large energy gains (up (o 20 times their original energy) in only a few such encounters with the shock. in some of these cases, the ions were kept near the shock by scattering and the very large magnetic fluctuations near the shock front, evident in Fig. 1 b, probably play a major role. The plot on the left in Fig. 3 is one such orbit. At the first encounter with the shock, the ion moves nearly along the shock front gaining energy from shock drift acceleration to E - $4X10^{-6}$. It then 1I1OVC.S upstream about 120 $c/\omega_{pi} \sim 14\ \rho_i$ where it is then scattered back to the shock for a second encounter and energy gain. in about 60% of the cases, the ions gained their energy in one or two such encounters. In the other -4(Y% of the cases studied, the ions moved a larger (> 100 c/ω_{pi}) distance from the shock before being scattering back or the energ y gain came from three or more encounters. An orbit of this type is shown on the right in Fig. 3. The ion has gained 24 times its original energy, corresponding to an increase from 240 eV to 6 keV. Note that our conclusion regarding the importance of shock drift acceleration relative to first order Fermi acceleration has been obtained using a model which includes no cross field diffusion. It is possible that cross-field diffusion could affect the accelerated ion orbits more than the simple linear estimate in Sec. 2 suggests.

The energetic particle flux resulting from the acceleration processes and the

diffusive shock theory predictions (straight lines) are shown in Fig. 4 for both Case 1 and Case 2 (below). Plotted is the flux spectrum or differential energy flux dJ/dE of the energetic/reflected ions in a region of width $300\, c/\omega_{pi}$ just ahead of the shock with energy normalized to the incident solar wind energy $\frac{1}{2} m V_{SW}^2$ 1:01' Case 1, many ions have been accelerated to more than 20 times the initial pick-up ion energy (E>6 keV).

Also shown in Fig. 4 is the slope of the flux predicted by diffusive shock theory

$$\frac{dJ(E)}{dE} \propto E^{-\alpha} \quad \text{with} \quad \alpha = \frac{r+2}{2(r-1)},$$

where r is the density compression ratio of the shock. Averaging over the very large fluctuations at the shock front, the observed density compression ratio for Case 1 is approximately $r \approx 3.2$ giving $\alpha \approx 1.2$, The slope predicted by diffusive shock theory is independent of the value of the diffusion coefficient and independent of the shock angle [Jones and Ellison, 1985; Baring et al., 1993]. The theory make no prediction of the magnitude of the differential flux. Moreover, diffusive shock theory is strictly applicable only for isotropic distribution functions and particles with velocities much higher than the convective velocities, and these conditions are certainly violated for the pick-up ion distributions in the simulation.

It is not clear how well the flux from the simulation should agree with the diffusive theory prediction. The flux from the simulation is clearly not a power law and there are several reasons for this, but there is some agreement with the slope predicted by diffusive theory in the mid-energy range where additional spatial ant] temporal variations expected in the simulated flux are less important. The above diffusive theory prediction is for the flux behind the shock, whereas we have plotted the upstream flux. Diffusive shock theory predicts that the upstream density of energetic ions should decay exponentially with distance from the shock front with the decay length increasing with ion energy [see review by Forman and Webb, 1985]. This was studied in the simulation of Giacalone et al. [1993] and, qualitatively, has been observed in these simulations as well. The much more rapid

fall off of the simulation flux than the diffusive theory prediction is due in part to the finite length and time of the simulation. Higher energy particles have a longer scattering mean free path and take longer simulation boxes and times to accelerate them.

3.2 *Case* 2 (θ_{Bn}= 50° *and MA* = 8)

For this case with θ_{Bn}= 50° and M_A = 8, the shock is much stronger and the ion energies are corresponding larger. However, many aspects are similar to Case 1. Figure 5 shows, for a time late in the simulation, the y component of the magnetic field $B_y(x)/B_0$, the total magnetic field strength $B(x)/B_0$ and the "energetic/reflected" pick up ion density n^P_{ref} normalized to the upstream pick-up ion density n^P_0, where, as above, "energetic/reflected" ions are those with 4 times the initial pick-up ion energy in the solar wind frame. The upstream waves have a somewhat larger amplitude as expected for this higher Mach number shock with more energetic pick-up ions. Note that some of the waves have steepened into "shock] lets." Very large amplitude ($\Delta B/B_0 \approx 8$) waves are also evident just downstream of the shock. The "energetic/reflected" density illustrates the efficiency of the shock acceleration process. In the region just upstream of the shock, the density of the energetic/reflected pick-up ions is very high (about 25% of the incident pick-up ion density just upstream). At earlier times ($t \approx 200\omega_{ci}^{-1}$), the reflected pick-up ion flux was large, $(n^PV)_{ref}/n^P_0V_{SW} \approx 40\%$ where here reflected ions are all pick-up ions moving to the left faster than the shock and where $(n^PV)_{ref}$ is calculated in the shock frame.

The higher Mach number relative to Case 1 leads to an upward shift in the bulk energy of the accelerated particles. The energetic particle differential flux resulting from the acceleration processes and the diffusive shock theory prediction for Case 2 are also shown in Fig. 4. Since the energies are normalized to the incident solar wind energies in Fig. 4 (240 eV in Case 1 and 611 eV in Case 2), the upward shift in energy is not readily apparent. Although the shape of the flux curves for the two cases are quite similar, the more energetic Case 2 is somewhat broader, extending to nigher relative energies. in Case 2, many ions have been accelerated to more than 50 times their initial energy (E>30 keV).

The broadening of the spectrum may be the result of a slightly slower fall off in energy for this case, consistent with the prediction of diffusive shock theory. For this case the average observed shock density compression ratio was $r \approx 3.4$ giving $\alpha \approx 1.1$ as compared to $r \approx 3.2$ and $\alpha \approx 1.2$ for Case 1. in the mid-energy range, the observed flux is consistent with the diffusive prediction although, as above, the flux from the simulation has additional spatial and temporal variations folded into the curve.

Figure 6 shows the magnetic fluctuation spectra $P(k) = B^2(k)/8\pi$ vs k, (with k in units of c/ω_{pi}) at two times in the simulation, $t\omega_{ci} = 150$ and 500, again integrated over a region extending 1024 c/ω_{pi} ahead of the shock. At the early tire, the spectrum is peaked in the region $ck/\omega_{pi} \approx$ 0.07-0.09. This is consistent with predictions for the beam-driven ion cyclotron instability for the observed reflected beam velocity of $V_b/V_A \approx$ 18-22. At later times, the spectrum has clearly broadened, with more energy going into longer wavelength modes as observed for Case 1 (Fig. 2). The broad enhancement in the spectral region $ck/\omega_{pi} \approx$ 0,02 --0.1 is presumably driven by the higher energy reflected pickup ions accelerated by this $M_A = 8$ shock.

Figure 7 shows the orbits of two of the most energetic pick-up ions from Case 2, energy (normalized to $m_p c^2/2$) versus distance from the shock (in units of c/ω_{pi}). Both ions have been accelerated to about 50 times their initial energy ($E_0 = 1.3 \times 10^{-6}$ or ~0.6 keV) to about 30 kcV. A study of 65 of the orbits of the most energetic ions for this case led to the same conclusions as for Case 1, i.e., the acceleration resulted primarily from shock drift acceleration in the shock front with the upstream waves aiding the processes by returning the ions to the shock for multiple encounters. Scattering from downstream waves was less important, Many ions studied appear to remain trapped near (within 100 c/ω_{pi}) the shock front (either by the fluctuations or the DC fields), acquiring their energy (via shock drift acceleration) in a small number of encounters with the shock. As in Case 1, in about 60% of the orbits studied, the ions had only one or two such encounters with the shock. In the orbit on the left in Fig. 7, the energy gain comes from shock drift acceleration in two

"encounters" with the shock. The ion on the right gains its energy from about 4 encounters with the shock. It should be noted that any trapping near the shock front could be strongly influenced by three-dimensional effects.

Recently Bennett et al. 11994] have raised the issue of whether or not energy is adequately conserved in a hybrid code such as ours which uses a first-order time stepping algorithm. We do not monitor energy conservation in our code and thus do not know how well energy is conserved. I Iowever, in Bennett et al., lack of energy conservation in a first-order hybrid code manifested itself in larger (by more. than 30%) density compression ratios across the shock than predicted by the Rankine-I lugoniot jump conditions. Thus, as a check, we have compared observed compression ratios with those predicted by the jump conditions for the same angle, Mach number and plasma beta. For the above cases, we computed the jump conditions and density compression for a shock moving with the observed speed using an ion β which includes the (dominant) contribution from the pick-up ions. For Case 1, the predicted density compression was 3.() and, averaging over the large oscillations, the observed ratio was $r \approx 3.2 \pm 0.2$. For Case 2, the predicted ratio was r = 3.2 and the observed ratio was $r \approx 3.4 \pm 0.3$. The large uncertainty in the compression ratio is due to the large oscillations at and behind the shock. Thus, the density compression exceeded the Rankine-I lugoniot prediction by at most about 10- 15% which is substantially less than the >30% seen by Bennett et al. using a first-order code.

3.3 Effect of Pick-up Ion Distribution Function

In Cases 1 and 2 above, the injected pick-up hydrogen velocity distribution function was a zero-thickness shell distribution with radius V_{SW}, co-moving with the solar wind. Mathematically, $f(v) \propto \delta(v - V_{SW})$ where v is in the solar wind frame.. This would *represent* the distribution function if all the ions were picked-llp anti isotropized in the vicinity of the termination shock. in fact, since the pick-up ions arc picked up throughout the heliosphere, the pick-up ions cool adiabatically due to the solar wind expansion as they travel out towards the shock, with those picked up farther in cooling more before reaching the shock.

'l-o test the sensitivity of the results to our choice of pick-up ion distribution function, we have also run smaller simulations using an adiabatically cooled distribution function $f(v) \propto v^{-3/2}$ for the range $v = (0, V_{SW})$ [Möbius et al., 1988], where, again, v is in the solar wind frame. This distribution represents a filled sphere of radius V_{SW} in velocity space, with $n(v)dv \propto f(v)v^2dv \propto v^{1/2}dv$, where n(v) is the angle-integrated pick-Lip ion velocity space density per unit shell width and n(v)dv *increases* with velocity up to the maximum $v = Vs_w$. Note that for this distribution, only about a third of the ions have a velocity less than $0.5V_{SW}$ in the solar wind frame.

simulations were run using the same parameters of Case 2, but on a smaller grid ($x_{max} = 1250\ c/\omega_{pi}$) for both the shell and the adiabatically cooled distribution functions and the resulting reflected pick-up hydrogen fluxes were compared. Results from both distributions are shown in Fig. 8 which plots the reflected pick-up hydrogen flux normalized to the incident hydrogen pick-up ion flux, $n_0 V_{SW}$, with both computed in the shock frame. Reflected pick-up ions were here defined as those moving upstream faster than the shock. The results are plotted at $t = 200\omega_{ci}^{-1}$, in the late "linear phase" so that the reflected flux could be evaluated before further wave scattering of the pick-ups back towards the shock becomes more significant. From Fig. 8, it can be seen that for the shell distribution, about 40% of the incident pick-Lip flux is reflected, **whereas** about 30% is reflected for the adiabatically cooled distribution. We have also compared the fluctuation spectra for these two cases and find that the power levels are similar, but with the shell (distribution having somewhat more power in longer wavelengths as expected. Thus, we conclude that the results presented in the preceding sections using a shell pick-up distribution rather than the adiabatically cooled pick-up distribution may overestimate the energetic fluxes by on the order of 30%. Generally speaking, however, the results are relatively insensitive to the two choices of injected pick-up ion distribution function.

3.4 *Comparison of Simulation Results with Extrapolated Voyager Energetic Particle Data*

The injection of interstellar pick-up ions into the macroscale global heliospheric

shock acceleration process is generally thought to occur primarily at the termination shock and not at interplanetary shocks because the termination shock is generally expected to be a much stronger shock and the acceleration time is inversely proportional to the' square of the Mach number (Jokipii, 1990). Moreover, interplanetary shocks are intermittent and confined to the vicinity of the current she-et. Here, we address this injection site issue by comparing the differential fluxes of the injected/accelerated pick-up hydrogen from our simulations with differential fluxes from interplanetary shock acceleration events measured by the LECP particle instrument cm Voyager, extrapolated to 80 AU, the termination shock location assumed in the simulations. If the flux of "seed" particles from interplanetary shocks at the termination shock location is greater than the fluxes injected locally at the termination shock itself (as predicted by the simulation), then interplanetary shocks would appear' to be a more important injection site. Since the interplanetary shock seed fluxis not measured at the location of termination shock, it is necessary to extrapolate the Voyager data.

Gold, Decker and Krimigis (1 988), hereafter GDK, plotted the differential fluxes (ions/cm^2-sec-keV-sr) in the keV-Mev range resulting from interplanetary shock acceleration as measured by the LECP instruments on Voyager 1 and 2. Wc have used the data from Fig. 4 of GDK as the basis for comparison. Specifically, wc. use the highest measured fluxes[curves (a) and (b) of GDK Fig. 4]. Curves (a) ant] (b) are averages of the eight largest shock accelerations events observed by LECP at Voyager 2 and 1 respectively during 1984 and early 1985 when Voyager . ? was about 15 AU and Voyager 1 was about 21 AU from the sun. The lower measured differential flux for shock acceleration events reported in GDK [curve (d) of Fig. 4] is lower than the highest flux by about a factor of about 6 in the lowest energy range (E ≈ 30 keV).

To compare with the simulation fluxes, the measured Voyager fluxes at R= 15 and 21 AU were extrapolated to the termination shock location, taken as 80 AU for the simulations. The extrapolation makes use of several assu options and introduces

considerable uncertainty in the comparison. We have performed the extrapolation to 80 AU using a simple adiabatic scaling of the energy range and fluxes with $\gamma = 5/3$. To do this, we take the measured flux in each energy "shell" dE and assume each shell extrapolates adiabatically between the measured location and 80 AU, e.g., $n \propto R^{-2}, E \propto R^{-4/3}, dE \propto R^{-4/3}$, flux $nV \propto R^{-8/3}$ and differential flux $d(nV)/dE \propto R^{-4/3}$. The most significant assumption in this extrapolation is that we neglect all production of flux into this energy range between 15 or 21 AU and 80 AU. We also neglect loss of flux in this range from acceleration to higher energies. Thus our extrapolation gives a fairly crude estimate of the value at 80 AU; interplanetary shocks will certainly continue to accelerate ions into this energy range. Note, however, this is the maximum flux measured by Voyagers 1&2; the average will be much less,

The extrapolated Voyager differential fluxes (ions/cm^2-sec-keV) are plotted in Fig. 9. The extrapolated Voyager 2 (R= 15 AU) flux (labeled V2) was calculated by scaling both the energy and the differential flux with radius (15/80)4/3 = 0.09; similarly the Voyager 1 (R=21AU) flux (V]) was scaled using $(21/80)^{4/3} = 0.17$.1'0 compare with the simulation fluxes, the LECP fluxes per steradian have been multiplied by 4π. Also shown in Fig. 9 are the simulation fluxes from Case 1, as well as fluxes from simulations for the same parameters as Case 1 ($M_A = 5, \theta_{Bn} = 40^o$), but higher Mach numbers ($M_A = 8$ and 10, as labeled in the plot). The large fluctuations in the spectra at high energies are due to the rather poor statistics. These could have. been improved by using particle. splitting techniques (e.g., Jones and Ellison, 1991; Giacalone et al., 1992).

From Fig. 9 it can be seen that the simulation fluxes for $M_A = 8$ are 1-2 orders of magnitude larger than the extrapolated Voyager fluxes. Note, however, that neither is a steady source. interplanetary shocks are generally confined to the region of the current sheet. Note also that the Voyager fluxes were for the largest shock acceleration events, and the average fluxes will be considerably lower. The simulation fluxes are obtained for termination shocks with $\theta_{Bn} < 60^o$, which applies about 10-30% of the time (see the

discussion in Sec. 2). The termination shock may also injects for $\theta_{Bn} < 60^{o}$, but the rate of injection at quasi-perpendicular shocks in at present unknown (see discussion in Sec. 2). We conclude that, given the 1-2 orders of magnitude difference, the termination shock is probably the more important site for injection and initial acceleration of the anomalous cosmic ray component than are interplanetary shocks,

4. Summary and Discussion

We have used a hybrid simulation model to show that interstellar pick-up hydrogen ions can be effectively injected and accelerated at the solar wind termination shock for oblique shock angles. The hybrid simulation model allows a self-consistent treatment of the shock fields, the solar wind and pick-up ions and the waves and turbulence. We have studied this process for oblique shocks in the range $\theta_{Bn} = 300$-600 and found qualitatively similar results. Reflected pick-up ions drive the strong upstream turbulence needed to support diffusive shock acceleration. At early times in the simulation, the spectrum is peaked at the mode expected for a reflected-ion-beam-driven ion cyclotron instability and the pick-up ion phase shows a well defined reflected beam. As the simulation progresses, the spectrum broadens in time with energy going to longer wavelengths as the pick-up ions are accelerated and non-linear wave scattering becomes important. For strong shocks ($M_A = 8$), many ions were accelerated to 50 times their initial energy, representing an increase from 0.6 keV to 30 keV for the parameters used. The magnitude of the "seed" energetic flux injected at the termination shock determined by the simulations was compared with measured energetic particle fluxes from Voyager extrapolated to the termination shock location. Although considerable uncertainty is introduced by the assumptions used in the extrapolation, the comparison suggests that the termination shock is a more important injection site than interplanetary shocks for the injection of the "seed" population for the anomalous cosmic ray component, Thus the results presented here provide a verification, on a microscopic scale, of the chain of processes by which interstellar pick-up ions can be reflected, accelerated locally and injected into the macro-scale global heliospheric diffusive

acceleration process which can further accelerate them to anomalous cosmic ray energies.

in this paper, injection was studied for termination shock angles $\theta_{Bn} < 60^o$ because injection occurred only for such angles in our 1D hybrid model. This model inherently neglects cross field diffusion. It may be that perpendicular diffusion can lead to significant injection for $\theta_{Bn}>60^o$. If cross-field diffusion is large enough to allow significant injection for shocks with $\theta_{Bn}>60^o$, them injection of pick-up ions from quasi-perpendicular shocks might be more important because the termination shock will be quasi-perpendicular more often than it is oblique. Because of these considerations, our calculations may underestimate the rate of injection of pick-up ions at the termination shock.

A study of orbits of the most energetic pick-up ions in our simulations shows that the primary mechanism of energy gain is shock drift acceleration at the shock front, with the waves allowing the ions to make multiple encounters with the shock. "l'he energy gained via shock drift acceleration in a single encounter can be much greater than that gained from simple specular reflection from the shock front. 1 n many cases, large energy gains resulted from only one or two interactions with the shock front. Scattering back to the shock from upstream waves was observed much more frequently than scattering from clown stream waves. For our simulations, the wave amplitude, and thus the diffusion coefficient, varies greatly with distance from the shock.

A comparison of results from two different Mach number simulations showed the energetic particle fluxes are qualitatively consistent with the predictions of diffusive shock theory, although diffusive theory is not strictly applicable to these simulations. At higher energies, the fluxes fall off more rapidly than the diffusive theory prediction. This is probably due to the finite length and time of the simulation. 7'0 run simulations large enough and long enough to accelerate particles to actual anomalous cosmic ray energies would be computationally prohibitive Rather-, the distribution of the energetic pick-ups fount] in micro-scale hybrid simulations can be used as the "seed" population to inject into macro-scale diffusive shock acceleration models which can than study the acceleration from

the tens of keV energies found here to the MeV anomalous cosmic ray range.

Acknowledgments. We wish to thank M. Lee and D. Ellison for valuable discussions and Edith 1 Iuang, JPL, for assistance in using the Delta. This work was carried out at the Jet Propulsion Laboratory, California Institute of Technology, under a contract with the National Aeronautics and Space Administration. The research was support in part by NASA/Heliospheric Physics and in part by NSF under Cooperative Agreement CCR-888W515. The computations were performed on the Intel Touchstone Delta parallel supercomputer operated for the Concurrent Supercomputing Consortium by the California Institute of Technology; access was provided by NASA.

References

Baring, M. G., Ellison, D. C., and Jones, F. C., The injection and acceleration of particles in oblique shocks: a unified Monte Carlo description, *Astrophys. J.*, 409, 327, 1993.

Bennett, L., Ellison, D. C., and Giacalone, J, Energy conservation in hybrid shock simulations (unpublished manuscript).

Baranov, V. B., and Malama, Yu. G., Models of the solar wind interaction with the local interstellar medium: numerical solution of seif-consistent problem, *J. Geophys. Res.* 98, 15157, 1993.

Burgess, D., Shock drift acceleration at low energies, *J. Geophys. Res.*, 92, 1119, 1987.

Decker, R. B., and Vlahos, 1.., Modeling of ion acceleration through drift and diffusion at interplanetary shocks, J. *Geophys. Res.*, 91, 13349, 1 986a.

Decker, R. B., anti Vlahos, I.., Numerical studies of particle acceleration at turbulent, oblique shocks with an application to prompt ion acceleration during solar flares, *Astrophys. J., 306,* 710, 1986b.

Decker, R. B., The role of drifts in diffusive shock acceleration, *Astrophys. J., 324,* 566, 1988.

Frisch, P., Morphology anti ionization of the interstellar cloud surrounding the solar

system, *Science, 265,* 1423, 1994.

Forman, M. A., and Webb, G. M., Acceleration of energetic particles, in *Collisionless Shocks in the Heliosphere: A Tutorial Review, Geophys. Monograph 34,91,* (R. G. Stone and B. 'T'. Tsurutani, eds.) AGU, 1985.

Giacalone, J., Jokipii, J. R., and Kota, J., Ion injection and acceleration at quasi-perpendicular shocks, *J. Geophys. Res., 99,* 19,351, 1994.

Giacalone, J., Burgess, D., and Schwartz, S. J., Ion injection and acceleration at parallel shocks: comparisons of self-consistent plasma simulations with existing theories, *Astrophys. J., 402,* 550, 1993.

Giacalone, J., Burgess, D., and Schwartz, S. J., Hybrid simulations of protons strongly accelerated by a parallel collisionless shock, *Geophys. Res. Letters. 19,* 433, 1992.

Gloeckler, G., Geiss, J., Balsiger, H., Fisk, L., Galvin, A., Ipavich, F., Ogilivie, K., von Steiger, R., and Wilken, B., Detection of interstellar pick-up hydrogen in the solar system, *Science,* 261, 70, 1993.

Gold, R. E., Decker, R.B., and Krimigis, S. M., The latitude and radial dependence of shock acceleration in the heliosphere, *J. Geophys. Res.,* 93, 991, 1988.

Jokipii, J. R., Particle drift, diffusion, and acceleration at shocks, *Astrophys. J., 25S,* 716, 1982.

Jokipii, J. R., Particle acceleration at a termination shock, 1, Application to the solar wind and the anomalous component, J. *Geophys. Res.,* 91, 2929, 1986.

Jokipii, J. R., Rate of energy gain anti maximum energy in diffusive shock acceleration, *Astrophys. J., 313, 842,* 1987.

Jokipii, J. R., "I'he anomalous component of cosmic rays, in Physics *of the Outer Heliosphere,* 169, ed. by S, Grzedzielski and D. E. Page, COSPAR, Pergamon, Oxford, 1990.

Jokipii, J. R., Kota, J., and Giacalone, J., Perpendicular transport in 1- anti 2-dimensional shock simulations, *Geophys. Res. Lett., 20,* 1759, 1993.

Jones, F. C. and Ellison, D. C., The plasma physics of shock acceleration, *Space Sci. Revs.* 5s, 259, 1991.

Karmesin, S. R., Liewer, P. C., and Brackbill, J, U., Motion of the termination shock in response to an 11 -year variation in the solar wind, *Geophys.Res.Lett.*,(to be published, 1995).

Liewer, P. C., Goldstein, B. E., and Omidi, N., Hybrid simulations of the effects of interstellar pick-Lip hydrogen on the solar wind termination shock, *J.Geophys.Res.* *98*, 15,211, 1993.

Möbius, E., Klecker, B , Hovestadt, D, and Scholer, M., Interaction of interstellar pick-up ions with the solar wind, *Astrophys.& Space Sci.* 144, 487, 1988.

Pesses, M., Jokipii, J.R., uric! Eichler, D., Cosmic ray drift, shock wave acceleration, and the anomalous component Of cosmic rays, *Astrophys.J.Lett.*, *?46,* 1.85,198 *1.*

Scholer, M. Diffuse ions at quasi-parallel collisionless shocks: simulations, *Geophys.Res. Lett., 17,* 1821, 1986.

Winske, D., and Leroy, M. M., Hybrid simulations techniques applied to the earth's bow shock, in *Computer Simulation of Space Plasmas--Selected Lectures at the First 1SSS,* ed. by H. Matsumoto and T. Sato, D. Ridel, 1 Iingham, Mass., 1985.

Figure Captions

Fig. 1. Results from Case 1 (θ_{Bn}= 40° and M_A = 5) at times early (a) and late (b) in the simulation. (a) Magnetic field y component $B_y(x)/B_0$ vs. x, pick-up ion v_x vs. x phase space (only every 60th particle plotted), and "energetic/reflected" pick up ion v_x vs. x phase space where "ctlcrgetic/reflected" pick-up ions are upstream ions with energy greater than 4 times the initial energy in the solar wind frame.(all plotted). The upstream wave structure can be clearly seen in both B_y and the phase space of the "energetic/reflected" pick-up ions, which drive the waves.(b) As in (a) except middle panel is magnitude of the total field vs. x.

Fig. 2. Power spectrum of the magnetic field fluctuations $P(k) = B^2(k)/8\pi$ vs k for Case at times early and late in the simulation with k in units of ω_{pi}/c. The peak at early times agrees with predictions for a reflected pick-Lip ion beam-driven ion cyclotron instability.

Fig. 3. "Orbits" of two ions from Case 1. Plotted is the ion's energy ($E = v^2/c^2$ in the solar wind frame) as a function of its distance from the shock front $x - x_{shock}$ (negative values are upstream). The ion position and energy (E_0=5x10^{-7}) at the start of the. simulation are at the bottom left end of the curve. The energy gain from shock drift acceleration is evident: the ions drift in the shock front ($x - x_{shock} \approx 0$) and gain energy continuously.

Fig. 4. Energetic ion fluxes resulting from the acceleration processes and the diffusive shock theory predictions for Case 1 (α=1.2) and Case 2 (α=1.1). Plotted is the spectrum or differential energy fiux of energetic/reflected ions in a region of width 300 c/ω_{pi} just upstream of the shock with energy is normalized to the. incident solar wind energy (240 eV for Case 1 and 611eV for Case 2). The energetic flux resulting from the stronger shock (Case 2) leads to a somewhat broader distribution with a slower frill off with energy, consistent with diffusive theory predictions.

Fig. 5. Results from Case 2 (θ_{Bn}= 50° and M_A = 8) late in the simulation. Magnetic field component By(x)/B(), the total magnetic field strength B(x)/B() and the "energetic/reflected" pick up ion density n^P_{ref}, normalized to the upstream pick-up ion density n^P_0.

Fig. 6. Power spectrum of the magnetic field fluctuations $P(k) = B^2(k)/8\pi$ vs k for Case 2 at times early and late in the simulation with k in units Of ω_{pi}/c.

Fig. 7. "orbits'" of two ions from Case2. Plotted is the ion energy ($E=v^2/c^2$ in the solar wind frame) as a function of distance from the shock front $x-x_{shock}$ (negative values are upstream). Both ions have been accelerated to about 50 times their initial energy to E - 6x 10-5, corresponding to about 30 keV.

Fig. 8. Comparison of reflected pick-up ions fluxes normalized to the incident pick-up ion flux from simulations using two different initial pick-up iorr distribution functions at a time early in the simulations, The top panel is for a shell distribution function (showing about 40% reflection) and the lower panel is for a adiabatically cooled distribution (showing about 30% reflection) as described in the text. The reflected flux is the flux of pick-up ions moving upstream faster than the shock computed in the shock frame.. Parameters are as for Case 2 except the system size is smaller.

Fig. 9. Comparison of simulation fluxes for three Mach numbers (M_A = S, 8 and 1 0; all θ_{Bn}= 40°) with Voyager 1&2 fluxes from interplanetary shock events extrapolated adiabatically to 80 AU. Plotted from the simulations are the differential energy fluxes (ions/cm^2-sec-keV) of energetic/reflected ions in a region of width 300 c/ω_{pi} just upstream of the shock, labeled by Mach number. Although uncertainty is introduced by the extrapolation, the significantly larger simulation fluxes suggests that the termination shock is the dominant site for injection of interstellar pick-up ions into the global heliospheric acceleration process. Note that both are intermittent sources.

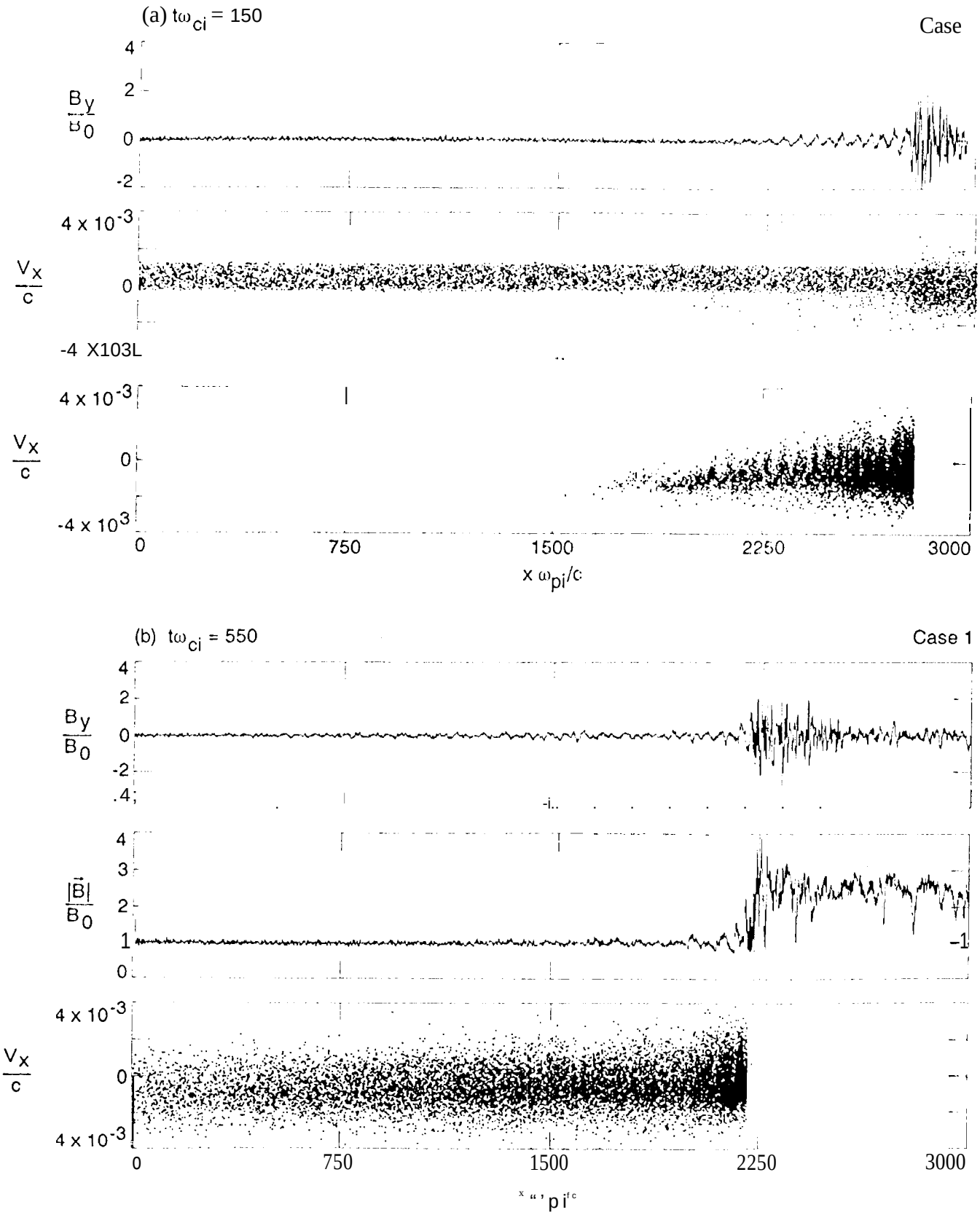
(a) tω_ci = 150
Case
B_y / B_0
V_x / c
4 x 10^-3
-4 X103L
0
750
1500
2250
3000
x ω_pi/c
(b) tω_ci = 550
Case 1
|B| / B_0
x ω_pi/c

Fig.]

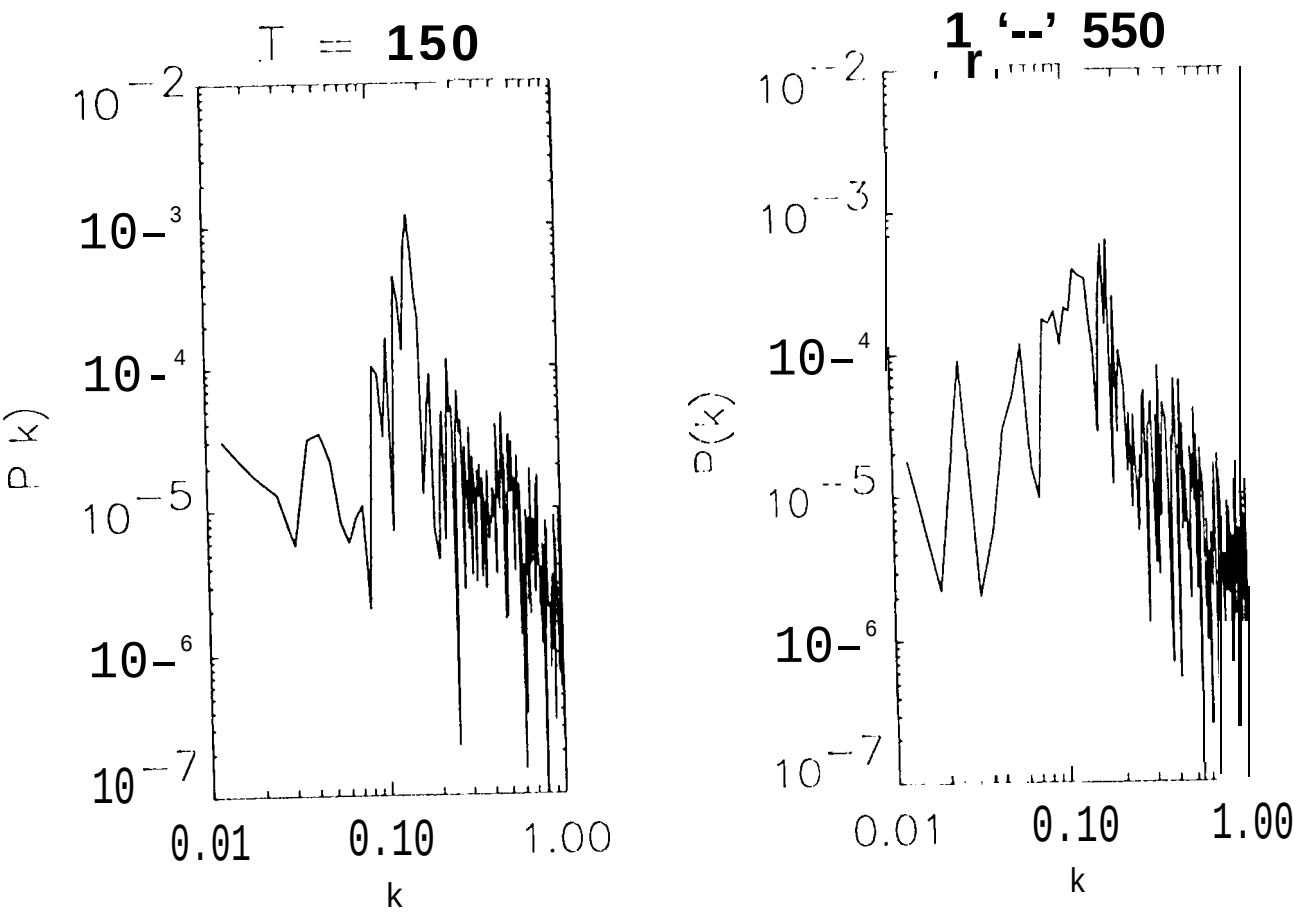
T = 150
10^-2
10^-3
10^-4
10^-5
10^-6
10^-7
P(k)
0.01
0.10
1.00
k
T = 550
10^-2
10^-3
10^-4
10^-5
10^-6
10^-7
P(k)
0.01
0.10
1.00
k

Fig. *2*

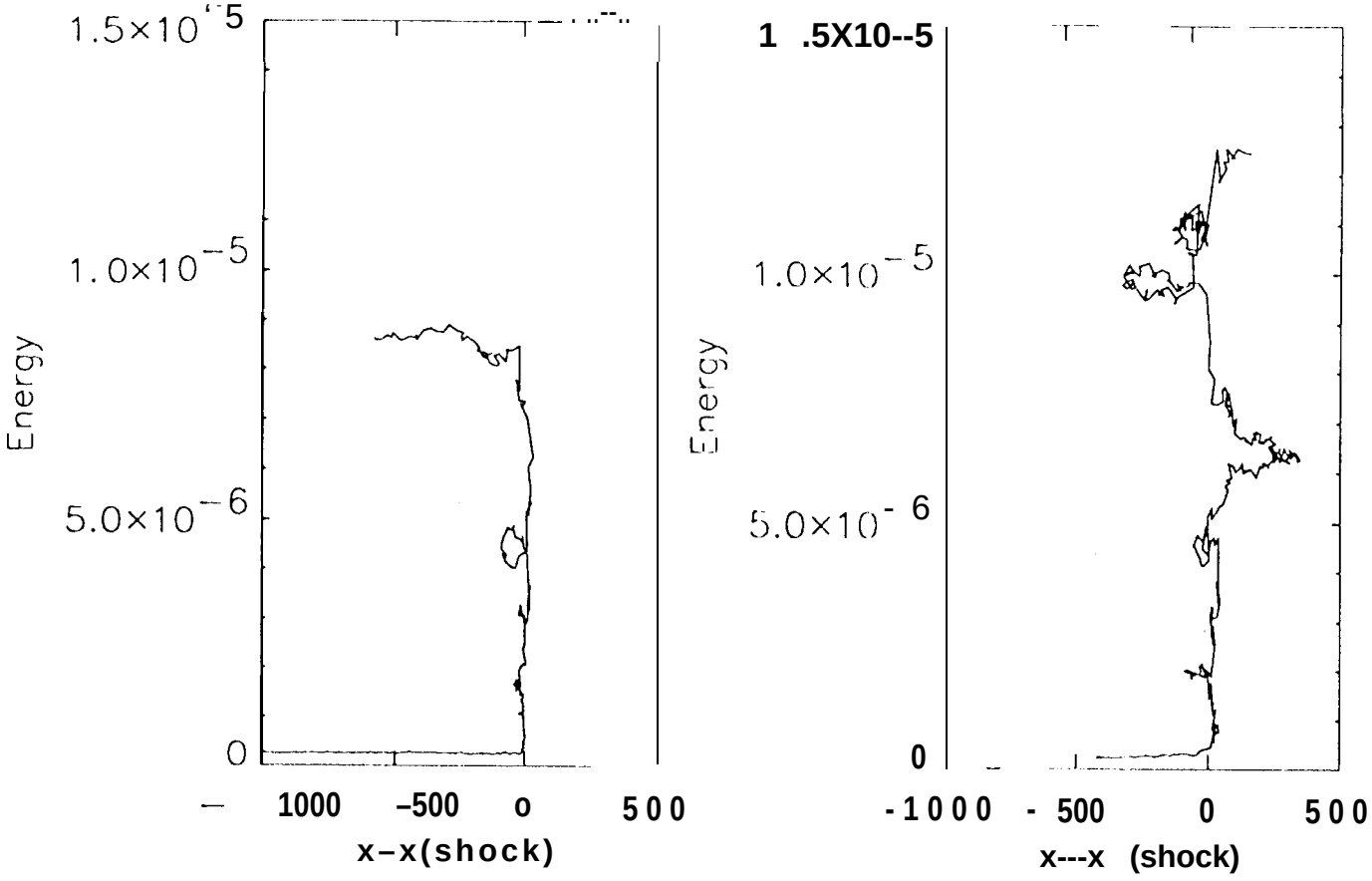
1.5×10⁻5
1.0×10⁻5
5.0×10⁻6
0
Energy
1000
–500
o
500
x–x(shock)
1 .5X10--5
1.0×10⁻5
5.0×10⁻6
0
Energy
-1000
- 500
0
500
x---x (shock)

Fig. 3

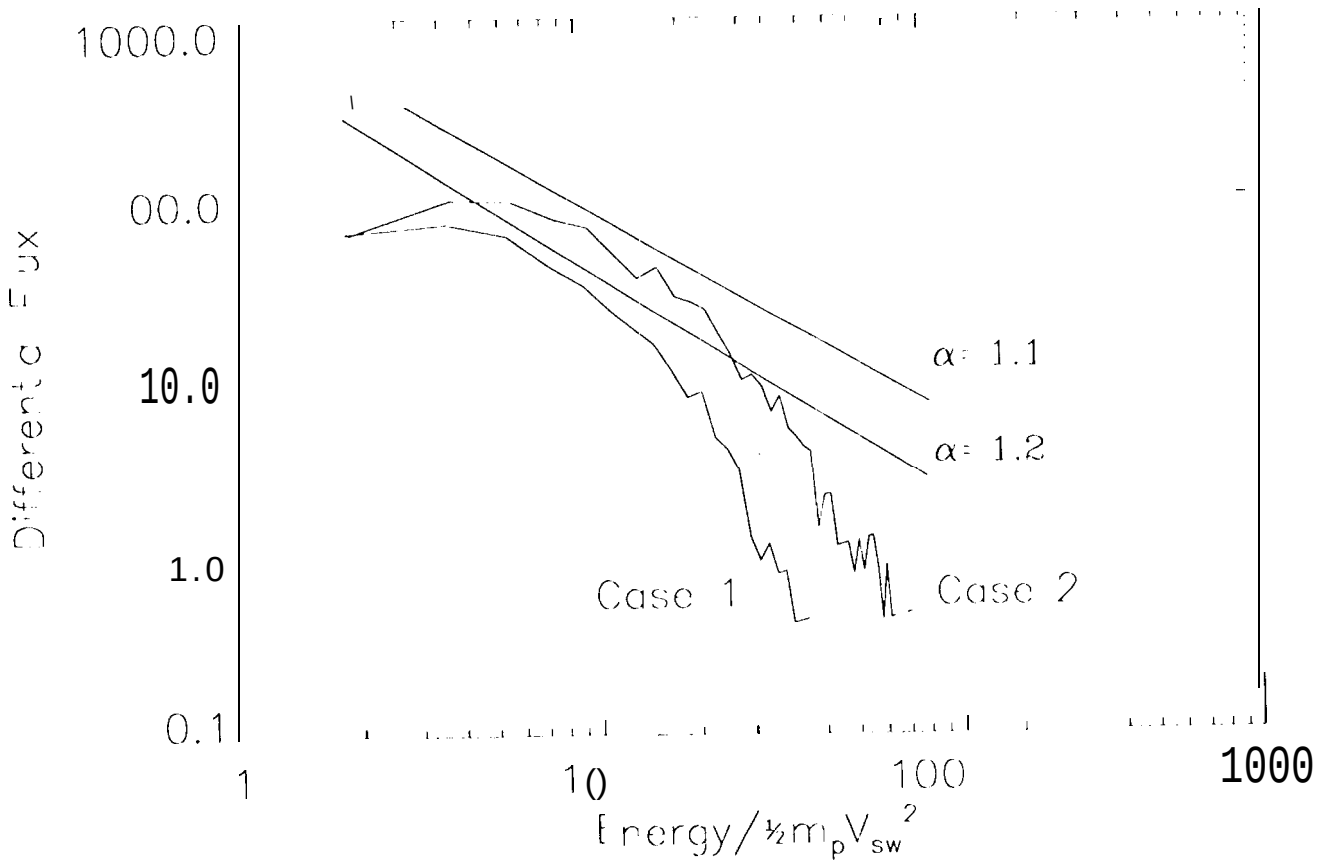
1000.0
00.0
10.0
1.0
0.1
Differential Flux
α= 1.1
α= 1.2
Case 1
Case 2
1
10
100
1000
Energy/½m$_p$V$_{sw}^2$

Fig. 4

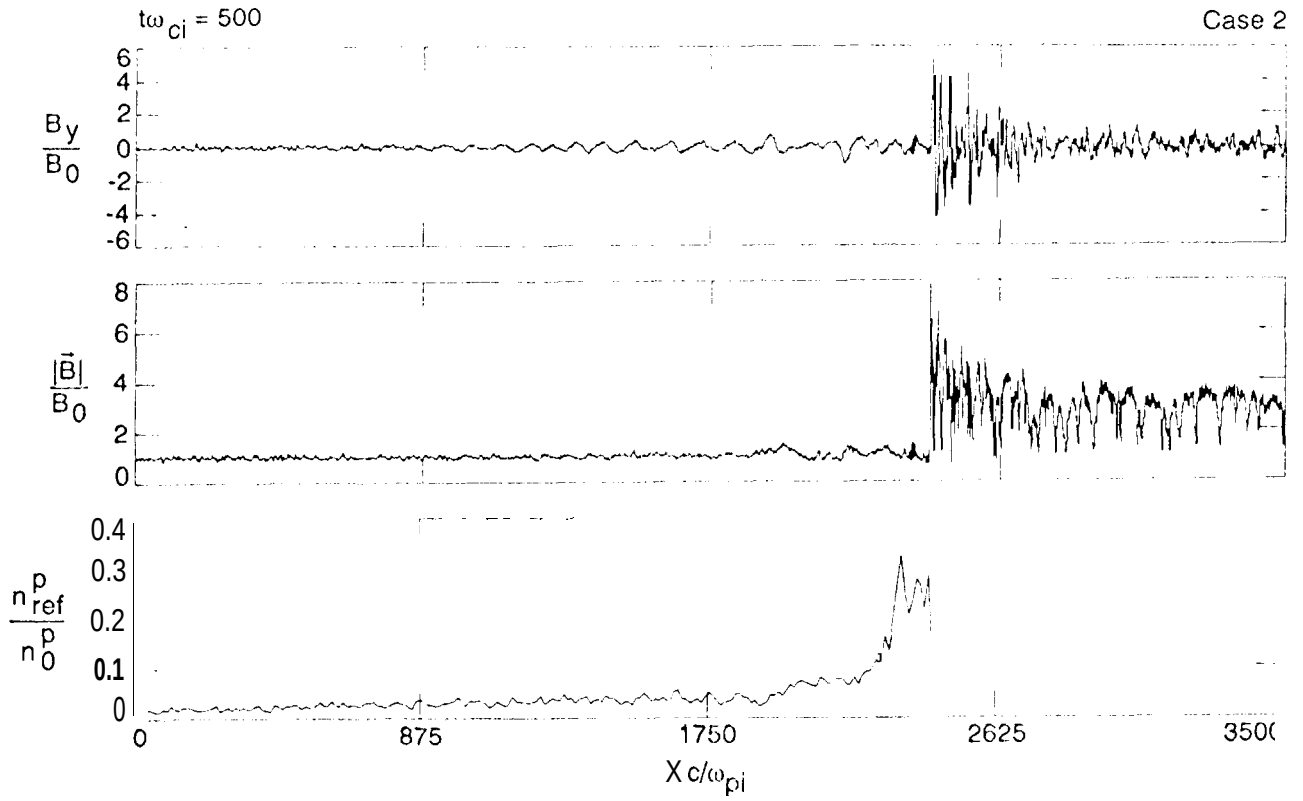

Fig. 5

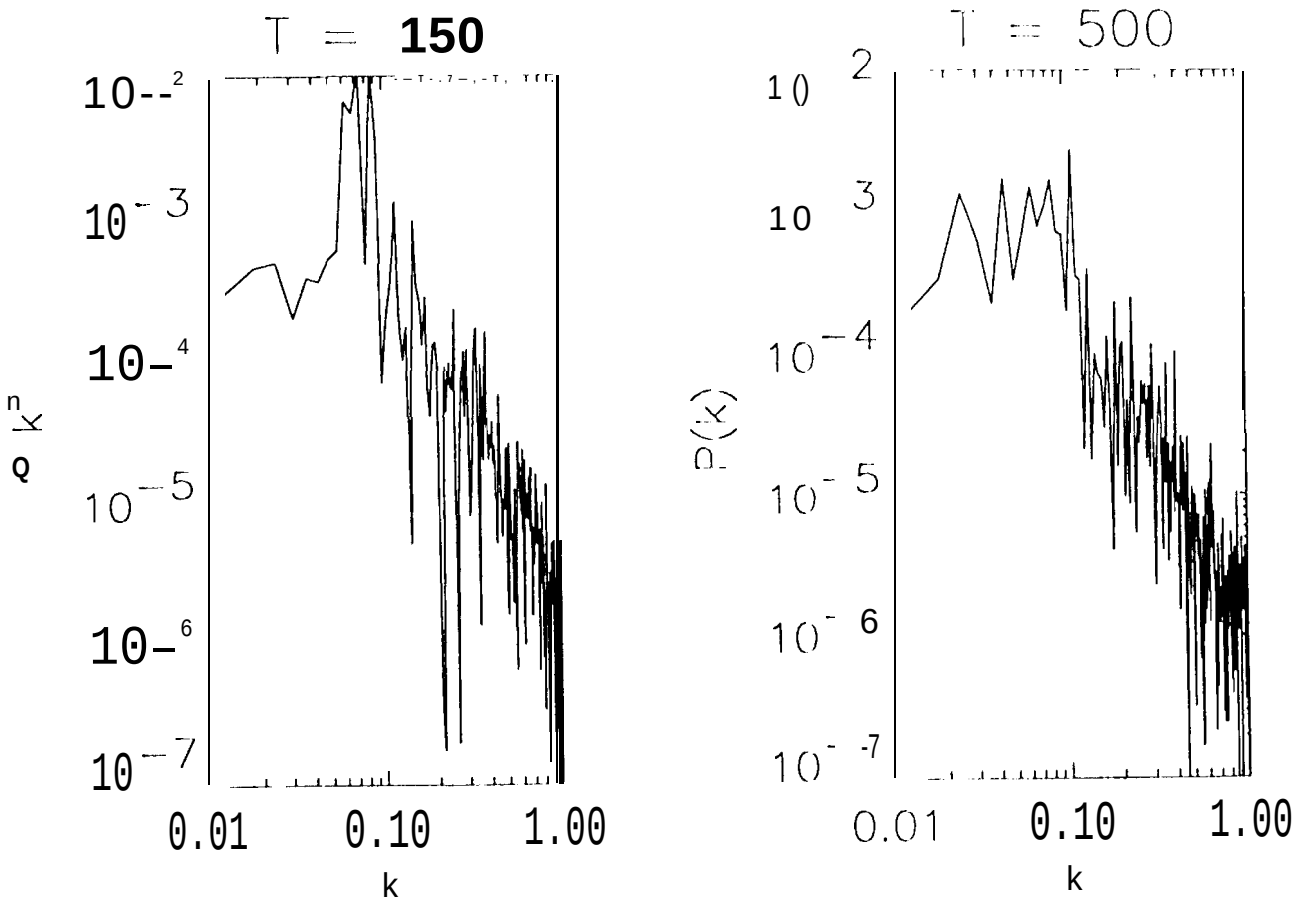
T = 150
10--2
10- 3
10-4
10-5
10-6
10-7
n
k
Q
0.01
0.10
1.00
k
T = 500
10 2
10 3
10-4
10- 5
10- 6
10- -7
n(k)
0.01
0.10
1.00
k

Fig. *6*

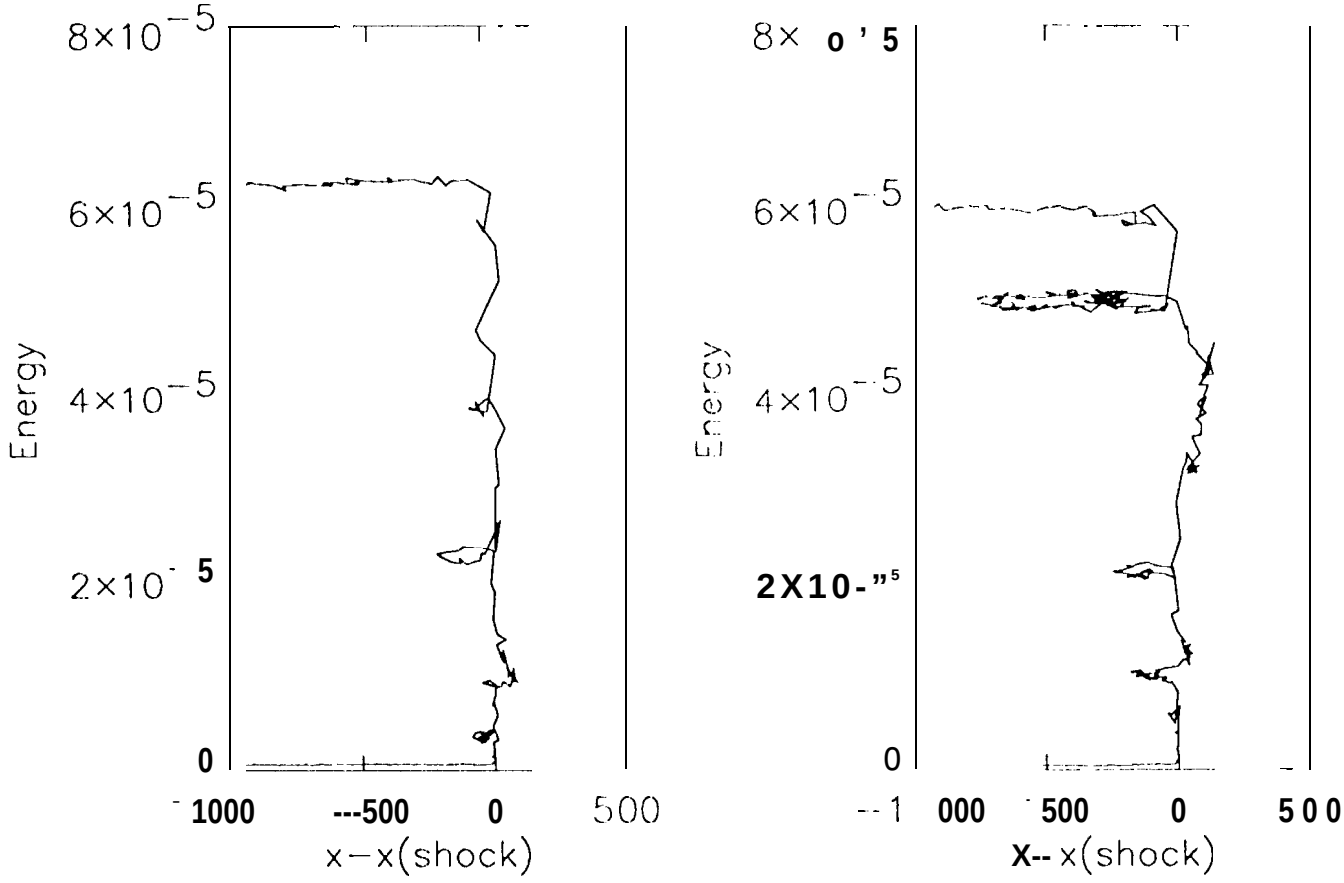
8×10⁻⁵
6×10⁻⁵
4×10⁻⁵
2×10⁻⁵
0
Energy
1000
---500
0
500
x−x(shock)
8×10⁻⁵
6×10⁻⁵
4×10⁻⁵
2X10-"⁵
0
Energy
1000
500
0
500
X-- x(shock)

Fig. 7

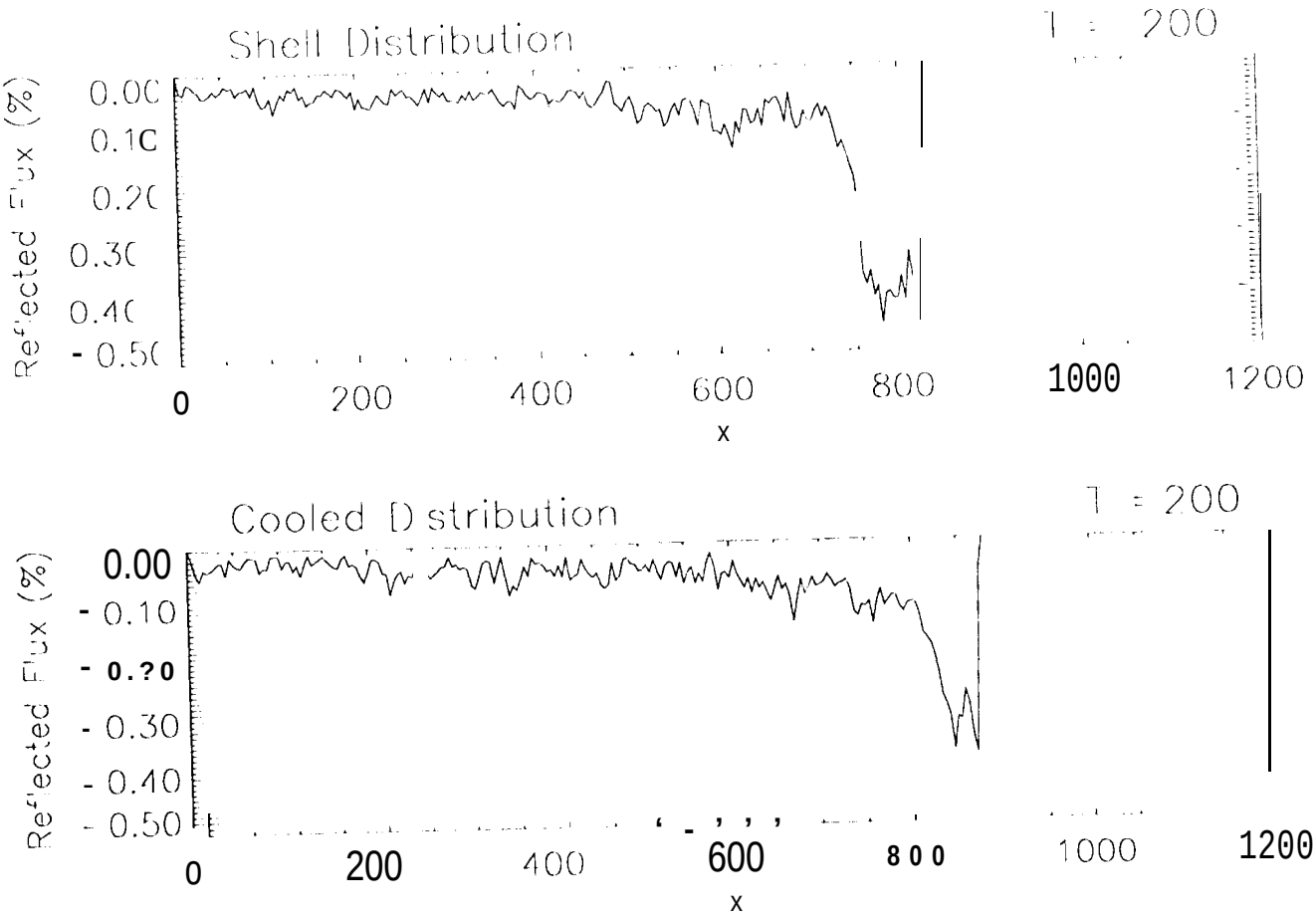
Shell Distribution
T = 200
Reflected Flux (%)
0.00
0.10
0.20
0.30
0.40
0.50
0
200
400
600
800
1000
1200
x
Cooled Distribution
T = 200
Reflected Flux (%)
0.00
- 0.10
- 0.20
- 0.30
- 0.40
- 0.50
0
200
400
600
800
1000
1200
x

Fig. 8

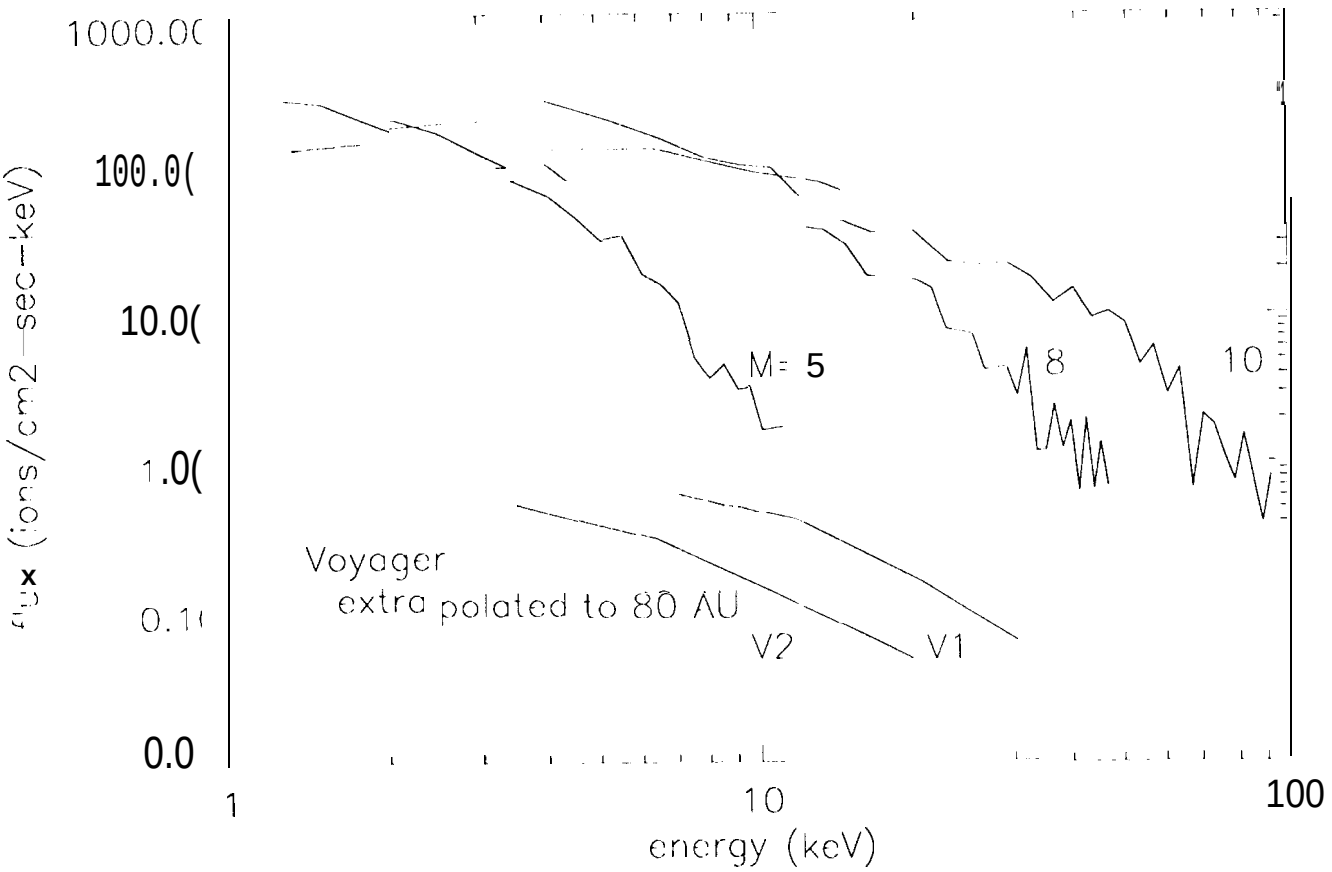
1000.0(
100.0(
10.0(
1.0(
0.0
1
10
100
energy (keV)
M= 5
8
10
Voyager
extrapolated to 80 AU
V2
V1

Fig. 9